JCTC Journal of Chemical Theory and Computation

Article

pubs.acs.org/JCTC

Elucidating the Electronic Structures of the Ground States of the $VO_2^{-/0}$ Clusters: Synergism between Computation and Experiment

Marc F.A. Hendrickx*,[†] and Van Tan Tran[‡]

[†]Afdeling Kwantumchemie en Fysicochemie, Departement Chemie, Katholieke Universiteit Leuven, Celestijnenlaan 200F, B-3001 Heverlee-Leuven, Belgium

[‡]Theoretical and Physical Chemistry Division, Dong Thap University, 783-Pham Huu Lau, Cao Lanh City, Dong Thap Vietnam

ABSTRACT: Electronic structures of VO_2 and its anion were investigated with density functional theory (DFT), complete active space second-order perturbation theory (CASPT2), and restricted coupled-cluster with single, double, and perturbative triple excitations (RCCSD(T)) computational quantum chemical methods. The results show that there is a near-degeneracy of the lowest $^3B_1$, $^3A_1$, and $^1A_1$ states of the anion. Therefore, the 532 and 193 nm photoelectron spectra of VO_2^- are interpreted by exploring these states as possible initial states. The anionic ground state was identified at the highest computational level, that is, RCCSD(T), as $^3B_1$ allowing the X band to be assigned to the $^3B_1 \rightarrow {}^2B_1$ transition, while the lower intensity and lower binding energy X′ and X″ features are ascribed to the $^1A_1 \rightarrow {}^2A_1$ and $^3A_1 \rightarrow {}^2A_1$ ionizations, respectively. The latter assignment is different from the recently proposed assignment of the corresponding slow electron velocity-map imaging (SEVI) spectra. Further, the A band is suggested to be mainly the result of an ionization from $^3B_1$ to 2^2A_1. For all these ionizations an electron is removed from a predominant metal orbital. The higher energy bands B and C on the contrary can be ascribed as electron detachments out of molecular orbitals largely located on the oxygen centers. More precisely, the B band is attributed to the ionizations from $^3B_1$ to $^4A_2$ and $^2A_2$, while the C band is proposed to originate from the $^3B_1 \rightarrow {}^4B_1$ and $^3B_1 \rightarrow 2^2B_1$ ionizations. The proposed novel assignment is further corroborated by calculating the Franck−Condon factors, which largely agree with the experimental vibrational progressions of the SEVI spectra.

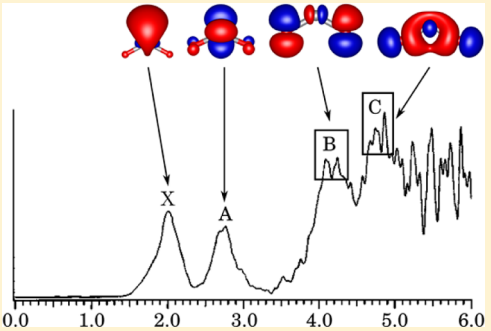

INTRODUCTION

Vanadium oxides have been known as very important materials for heterogeneous catalysis,[1−4] which makes the investigation of the nature of vanadium−oxygen bonds quite valuable. For this reason the structural and electronic properties of small vanadium oxide clusters have been studied extensively both by experimental and theoretical chemists.[5−17] In this work, we are interested in vanadium dioxide and its anion because these clusters exhibit very complicated electronic structures as a result of a partially occupied 3d shell of vanadium. For the neutral cluster, previous computational studies show a near-degeneracy of the $^2A_1$ and $^2B_1$ states, which is the result of a splitting of the linear $^2\Delta_g$ state under the Renner−Tell effect.[5−8] By using complete active space self-consistent field (CASSCF), BPW91, B1LYP, and CCSD(T) methods, the $^2A_1$ was predicted as the neutral ground state.[6−8] In contrast, the B3LYP functional identifies the $^2B_1$ as the lowest energy state.[5] For the anionic cluster, on the other hand, nearly degenerate $^3A_1$ and $^3B_1$ states, as components of the linear $^3\Delta_g$ state, were recognized as the lowest states.[6,8] Both BPW91 and B3LYP functionals compute the $^3A_1$ as the anionic ground states,[5,6] while the B1LYP functional and CCSD(T) place this state 0.06 and 0.19 eV higher than the $^3B_1$ state.[8] Recently, CASSCF and density functional theory (DFT) calculations with BPW91 and B3LYP functionals also confirmed the near-degeneracy of the neutral $^2A_1$ and $^2B_1$ and of the anionic $^3A_1$ and $^3B_1$ states.[18]

Experimentally, the electronic structures of these clusters have been investigated by using photoelectron spectroscopy.[9,18] In particular, the photoelectron spectra of VO_2^- have been reported for photon detachment energies of 532, 355, 266, and 193 nm.[9] The highest resolution 532 nm spectrum shows three features, that is, an X band at 2.03 eV with a clear vibrational progression of three sharp peaks that are 970 cm^{-1} apart. At the lower energy end two low-intensity features, labeled X″ feature at 1.90 eV and X′ feature at 1.72 eV, were recorded. The higher photon energy spectra also revealed A, B, and C bands at 2.60, 4.00, and 4.60 eV, respectively. By using the electronic structure data of previous theoretical studies of the neutral cluster,[7,9] the authors assumed a $^1A_1$ with a closed-shell electronic configuration as the anionic ground state. Consequently, the X, A, B, and C bands in the spectra were assigned by using this singlet state as the initial state, while the X′ and X″ features were believed to be the result of ionizations from some low-lying excited anionic states. However, this proposed assignment is in contradiction with more recent computational results that point to a $^3A_1$ or a $^3B_1$ state as the ground state of VO_2^-.[5,6,8,18]

Received: June 17, 2014
Published: July 7, 2014

   dx.doi.org/10.1021/ct500526m | J. Chem. Theory Comput. 2014, 10, 4037−4044

Very recently, high-resolution photoelectron spectra of VO_2^- as obtained with slow electron velocity-map imaging (SEVI) of trapped and cryogenically cooled anions were also reported.[18] These spectra show three vibronic progressions starting at 1.8357 eV (X band), 2.0202 eV (A band), and 2.6487 eV (B band), respectively. When comparing these high-resolution photoelectron spectra with the previously reported photoelectron spectra,[9] it is clear that the X, A, and B bands correspond to the X″, X, and A bands, respectively. The X′ band in the original spectra does not appear in the recent high-resolution spectra. On the basis of their BPW91 Franck−Condon factor simulations and ignoring their B3LYP data, the X, A, and B bands were all ascribed to electron detachments from the anionic $^3B_1$ ground state to the neutral $^2A_1$, $^2B_1$, and 2^2A_1 states, respectively. It should, however, be noted that the $^3B_1 \rightarrow {}^2A_1$ ionization is not a one-electron detachment process and therefore should not been seen in the spectra, unless at least one of these states is of multireference character.

In summary, from previous theoretical and experimental studies, it can be concluded that the electronic structures of $VO_2^{-/0}$ are not unambiguously described yet, and consequently there is a necessity to study them with more accurate quantum chemical techniques. In this work, DFT, restricted coupled-cluster with single, double, and perturbative triple excitations (RCCSD(T)), and complete active space second-order perturbation theory (CASPT2) were applied with the purpose to determine the ground states of the $VO_2^{-/0}$ clusters and to identity the low-lying states of the neutral cluster, which are responsible for the observed bands in the anion photoelectron spectra. For these kinds of transition metal oxide clusters, CASPT2 has been demonstrated to be very efficient in locating the relative positions of all relevant electronic states,[19−21] while RCCSD(T) appears to be the superior method for identifying the relative stability of the ground states of closely lying isomers.[19,20] With this computational experience at hand, we propose assignments for all bands in the photoelectron spectra of VO_2^-. Franck−Condon factor simulations, which in the past were utilized successfully to reproduce the measured vibrational fine structures,[18−22] will also in the present case be proved to be of vital importance for performing the final assignment of the entire experimental spectra. Our assignments will use the labeling of the experimental bands as proposed by Wang and co-workers[9] and the labeling of the recent high-resolution SEVI spectra[18] next to each other. This will be indicated clearly throughout the text, but notice that the X″, X, and A bands in the 532 nm spectrum[9] correspond to the X, A, and B bands of the SEVI spectra.[18]

COMPUTATIONAL METHODS

Previous calculations considered three isomers for the stoichiometric VO_2 cluster, which were denoted as dioxide (VO_2), peroxide ($V(O_2)$), and superoxide (VOO).[6,8] Because the $V(O_2)^{-/0}$ and $VOO^{-/0}$ isomers were predicted by BPW91, B1LYP, and CCSD(T) to be at least 3 eV less stable than $VO_2^{-/0}$, only the latter clusters are studied in this work. The coordinate system for $VO_2^{-/0}$, as used in our calculations and depicted in Figure 1, places all three nuclei in the *yz* plane, while the C_2 axis of the C_{2v} point group is set to coincide with the *z* axis.

To identify all low-lying electronic states of $VO_2^{-/0}$, we performed CASPT2 calculations first. The molecular orbitals for CASPT2 were obtained from a CASSCF calculation with an active space comprising 13 or 14 electrons distributed among 12 orbitals, including the 3d and 4s of vanadium and the 2p orbitals of oxygen. At this level of theory the geometries were optimized by imposing C_{2v} symmetry. ANO-RCC basis sets with contractions [7s6p4d3f2g] and [5s4p3d2f] were employed for, respectively, vanadium and oxygen.[23,24] Scalar relativistic effects were included by using the Douglas−Kroll Hamiltonian.[25−27] For avoiding problems with intruder states, an imaginary shift of 0.1 was used. In addition to the valence electrons, our CASPT2 calculations also correlated the outer core 3s and 3p electrons of vanadium and the 2s electrons of oxygen. All CASPT2 calculations were performed with the MOLCAS 7.6 suite of programs.[28]

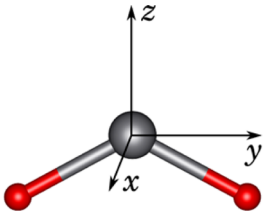

Figure 1. Coordinate system for the $VO_2^{-/0}$ clusters as used for the DFT, CASPT2, and RCCSD(T) calculations.

With the CASSCF leading electronic configuration of the relevant states firmly determined, we performed DFT and RCCSD(T) calculations. Both the hybrid B3LYP[29−31] and pure BP86[29,32] functionals in combination with the def2-QZVP[33] basis sets were employed in this work. Geometries of all low-lying states were optimized within the C_{2v} symmetry. Vibrational frequencies were calculated at the DFT level for the optimized structures to verify that they correspond all to minima on the potential energy surfaces. RCCSD(T) was applied as the most accurate method in this article. In this context the aug-cc-pwCV5Z-DK[34] basis sets were utilized for vanadium and oxygen. To recover the scalar relativistic effects, the Douglas−Kroll Hamiltonian to second order was used.[25−27] Similar to CASPT2, our RCCSD(T) calculations correlated the 3s, 3p, 3d, and 4s electrons of vanadium and the 2s and 2p electrons of oxygen. Geometries were optimized, and harmonic vibrational analyses were carried out manually. For this purpose the energy profiles for the symmetric stretching and bending modes were fitted to quadratic equations, which allowed the estimation of the force constants for the V−O bonds and O−V−O bending. On the basis of these RCCSD(T) geometries, harmonic vibrational frequencies, and corresponding vibrational normal modes, Franck−Condon simulations were carried out with the MOLFC code[35] to reproduce the vibrational progressions of the low-lying bands in the 532 nm photoelectron spectrum[9] and of the high-resolution SEVI spectra of VO_2^-[18]. All DFT and RCCSD(T) calculations were done with the MOLPRO 2009 program package.[36]

RESULTS AND DISCUSSION

The Low-Lying States of $VO_2^{-/0}$. The relative energies and geometries of the low-lying states of $VO_2^{-/0}$ as calculated by B3LYP, BP86, and RCCSD(T) are collected in Table 1. The same data obtained by CASPT2 together with the electronic configurations, adiabatic detachment energies (ADEs), and vertical detachment energies (VDEs) can be found in Table 2. Figure 2 depicts the corresponding molecular orbitals for the $^3B_1$ state. For the anionic structures, only the CASPT2 results allow the identification of all three nearly degenerate low-lying electronic states. Indeed, the maximum energy difference

dx.doi.org/10.1021/ct500526m | J. Chem. Theory Comput. 2014, 10, 4037−4044

Table 1. Structural Parameters, Relative Energies, and Vibrational Frequencies of the Low-Lying States of $VO_2^{-/0}$ Clusters

method	cluster	state	V−O[a] (Å)	OVO[a] (deg)	RE[a] (eV)	frequencies[a,b] (cm^{-1})
B3LYP	VO_2^-	$^3A_1$	1.655	124.42	0.06	287, 923, 925
		$^3B_1$	1.652	122.09	0.00	284, 923, 927
	VO_2	$^2A_1$	1.612	116.40	1.91	258, 1024, 934
		2^2A_1	1.596	113.43	2.83	415, 1023, 1039
		$^2B_1$	1.613	120.97	1.94	312, 1020, 1008
BP86	VO_2^-	$^3A_1$	1.658	121.36	0.10	291, 906, 907
		$^3B_1$	1.654	118.51	0.00	291, 908, 909
	VO_2	$^2A_1$	1.613	110.27	1.86	323, 998, 979
		2^2A_1	1.606	113.38	2.71	308, 1014, 1007
		$^2B_1$	1.622	118.66	2.03	314, 983, 980
RCCSD(T)	VO_2^-	$^3B_1$	1.651	122.09	0.00	321, 926, 1050
		$^3A_1$	1.654	123.70	0.02	285, 912, 1039
	VO_2	$^2A_1$	1.617	113.59	1.88	280, 984, 1080
		$^2B_1$	1.620	120.83	2.00	324, 986, 1112
		2^2A_1[c]			2.86	
		$^4A_2$[c]			4.31	
		$^4B_1$[c]			4.95	

[a]Calculated at the B3LYP, BP86, and RCCSD(T) levels. [b]Frequencies are shown in the order of the OVO bending, the symmetric V−O stretching, and the V−O asymmetric stretching modes. [c]Single-point calculations for the mentioned states at the geometry of the $^3B_1$ ground state of the anionic cluster. The relative energies therefore correspond to the vertical detachment energies.

Table 2. CASSCF Leading Electronic Configurations and CASPT2 Results

cluster	state	leading configuration	orb.[a]	V−O (Å)[b]	OVO (deg)[b]	RE (eV)[b]	VDE (eV)[b]	expt.[c] (eV)	expt.[d] (eV)
VO_2^-	$^1A_1$	$9a_1^2 10a_1^1 11a_1^1 4b_1^0 6b_2^2 1a_2^2$		1.641	109.88	0.03			
	2^1A_1	$9a_1^2 10a_1^0 11a_1^2 4b_1^0 6b_2^2 1a_2^2$		1.659	120.52	1.06			
	$^3A_1$	$9a_1^2 10a_1^1 11a_1^1 4b_1^0 6b_2^2 1a_2^2$		1.666	122.35	−0.07			
	$^3B_1$	$9a_1^2 10a_1^0 11a_1^1 4b_1^1 6b_2^2 1a_2^2$		1.663	122.87	0.00	0.00		
	$^1B_1$	$9a_1^2 10a_1^0 11a_1^1 4b_1^1 6b_2^2 1a_2^2$		1.665	122.75	0.34			
VO_2	$^2A_1$	$9a_1^2 10a_1^1 11a_1^0 4b_1^0 6b_2^2 1a_2^2$	$11a_1$	1.613	105.80	1.62[e]	1.88	1.90 (X″)	1.84 (X)
	$^2B_1$	$9a_1^2 10a_1^0 11a_1^0 4b_1^1 6b_2^2 1a_2^2$	$11a_1$	1.635	119.92	1.75[f]	1.78	2.03 (X)	2.02 (A)
	2^2A_1	$9a_1^2 10a_1^0 11a_1^1 4b_1^0 6b_2^2 1a_2^2$	$4b_1$	1.625	117.95	2.16[f]	2.27	2.60 (A)	2.65 (B)
	$^4A_2$	$9a_1^2 10a_1^0 11a_1^1 4b_1^1 6b_2^1 1a_2^2$	$6b_2$				4.14	4.00 (B)	
	$^4B_1$	$9a_1^1 10a_1^0 11a_1^1 4b_1^1 6b_2^2 1a_2^2$	$9a_1$				4.58	4.60 (C)	
	$^2A_2$	$9a_1^2 10a_1^0 11a_1^1 4b_1^1 6b_2^1 1a_2^2$	$6b_2$				4.12	4.00 (B)	
	2^2B_1	$9a_1^1 10a_1^0 11a_1^1 4b_1^1 6b_2^2 1a_2^2$	$9a_1$				4.55	4.60 (C)	

[a]The column denoted orb. specifies the orbitals from which an electron is removed for the corresponding assignation as mentioned in the columns denoted expt. (for details see text). [b]Structural parameters, relative energies (REs), and vertical detachment energies (VDEs) from the $^3B_1$ state as obtained at the CASPT2 level. [c]Experimental data according to ref 9. [d]Experimental data according to ref 18. [e]Adiabatic detachment energy from the $^3A_1$ anionic first excited state. [f]Adiabatic detachment energy from the $^3B_1$ anionic ground state.

between the $^3B_1$, $^3A_1$, and $^1A_1$ is less than 0.1 eV, with the $^3A_1$ as the lowest state. The DFT and RCCSD(T) data in Table 1 confirm the near degeneracy of the $^3B_1$ and $^3A_1$ states, with an energy difference between that is also less than 0.1 eV. However, the latter method identifies the $^3B_1$ as the ground state of the anion. As single-determinant computational techniques, RCCSD(T) and both DFT methods cannot calculate the $^1A_1$, since Table 2 shows that it is the lower spin state of the same configuration as the $^3A_1$. Because of the larger exchange energy, the former state is expected at a somewhat higher energy than the latter, which is indeed confirmed in Table 2 at the CASPT2 level by placing the $^1A_1$ 0.10 eV higher than the $^3A_1$. On the other hand, the closed-shell 2^1A_1 state is located at much higher energies of about 1 eV above the open-shell $^1A_1$ state, allowing the elimination of this state definitely as a possible ground state. On the contrary, because of the small energy difference between $^3B_1$, $^3A_1$, and $^1A_1$, it is impossible to eliminate any of them as the anionic ground state. This finding explains why, in the literature, different ground states are reported for VO_2^-.[5,6,8,18] In most studies, the anionic ground state was computed to be the $^3A_1$[5,6] or the $^3B_1$ state,[8,18] while no reference to the open-shell $^1A_1$ state was made. In view of our past experience with similar types of clusters,[19,20] we are inclined to accept the RCCSD(T) results of Table 1 and to predict the $^3B_1$ state as the ground state of VO_2^- and therefore as the initial state for the higher-intensity bands of its photoelectron spectra, that is, bands X and A to C of the 193 nm spectrum in Figure 3. The underlying reason for this being the superior capacity of this computational method to recover the dynamical correlation energy, which appears of principal importance to identify the ground states of transition metal-containing clusters. Accepting the $^3B_1$ state as the ground state therefore leads to the high-spin state $^3A_1$ as the first excited state and the corresponding low-spin state $^1A_1$ of the same electronic configuration as the second excited state of the anionic VO_2^-.

dx.doi.org/10.1021/ct500526m | J. Chem. Theory Comput. 2014, 10, 4037−4044

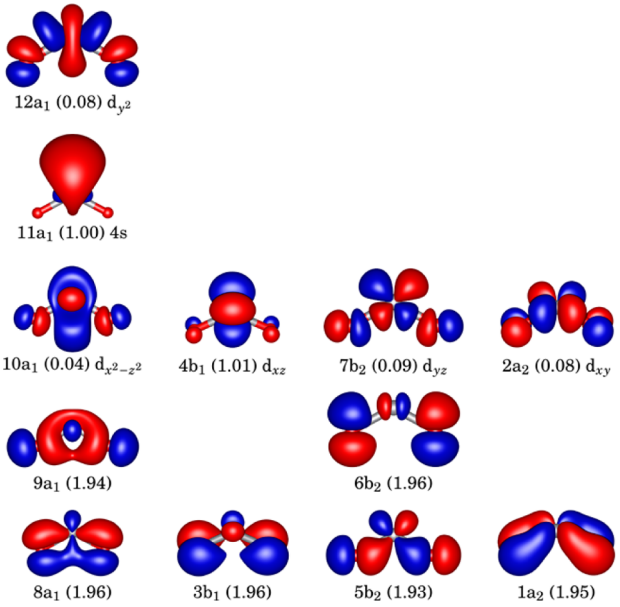

Figure 2. Pseudonatural CASSCF orbitals of the $^3B_1$ state of VO_2^- and their natural occupation numbers ordered according to their symmetry properties.

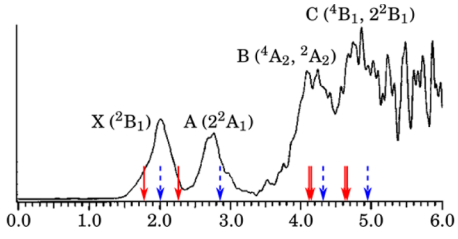

Figure 3. 193 nm photoelectron spectrum[9] of VO_2^-. The red (solid) and blue (dashed) arrows represent the vertical detachment energies as calculated at the CASPT2 and RCCSD(T) levels, respectively. Abscissa: binding energy in eV. Ordinate: arbitrary units for intensities.

For the neutral VO_2 cluster, we find a near-degeneracy for the two lowest states, namely, $^2A_1$ and $^2B_1$. All the computational methods employed in this work predict the $^2A_1$ as the ground state. However, at the CASPT2 level, the $^2B_1$ is positioned just 0.13 eV higher. At the B3LYP and BP86 levels, this energy gap between them is reduced to 0.03 and 0.17 eV, respectively. The more accurate RCCSD(T) calculations predict a value of 0.12 eV for this gap. With this small energy difference, it is impossible to identify unambiguously the true ground state of VO_2. This can be seen in previous computational studies where the neutral ground state is occasionally predicted as the $^2A_1$ state[6−8,18] or the $^2B_1$ state.[5] In addition to the $^2B_1$ state, the second excited state, namely, the 2^2A_1, is computed to be 0.54 eV higher than the $^2A_1$ ground state by CASPT2. At the B3LYP, BP86, and RCCSD(T) levels, this state is destabilized and is calculated as much as 0.92, 0.85, and 0.98 eV higher than the $^2A_1$ state, respectively. Overall, our computational results show a small splitting for the low-lying states of the anionic and neutral clusters, which are smaller than the expected error bar of the employed methods. Thus, to establish the true ground states with greater certainty, it is necessary to make use of the available information on the experimental photoelectron spectra of VO_2^-, that is, detachment energies and vibrational structure of the various bands. For doing so, the application of the one-electron detachment rule is of vital importance, which implies a thorough knowledge of the electronic structures of all states involved.

The Electronic Structures of $VO_2^{-/0}$. The leading electronic configurations of the low-lying states as obtained from CASSCF are shown in Table 2. The pseudonatural molecular orbitals of the $^3B_1$ (lowest energy state) of VO_2^- are represented in Figure 2, where it can be seen that the predominantly 3d and 4s orbitals of vanadium can be divided into two groups: the nonbonding $10a_1$ ($3d_{x^2-z^2}$), $11a_1$ (4s,4p), and $4b_1$ ($3d_{xz}$) orbitals, and the antibonding $12a_1$ ($3d_{y^2}$), $7b_2$ ($3d_{yz}$), and $2a_2$ ($3d_{xy}$) orbitals. Among these, the $11a_1$ (4s,4p) and $4b_1$ (d_{xz}) orbitals are singly occupied, while the remaining d orbitals are unoccupied. All the orbitals of oxygen, that is, the $9a_1$, $5b_2$, $8a_1$, $3b_1$, $6b_2$, and $1a_2$, are doubly occupied. From the $^3B_1$ state, the other low-lying anionic electronic states can be obtained by one electron transfer processes. The $^3A_1$ can be obtained by transferring the unpaired electron from the $4b_1$ orbital to the $10a_1$ orbital. The electron configurations of the $^3A_1$ and $^3B_1$ in Table 2 show that these states originate from the linear $^3\Delta_g$ state as the result of Renner−Teller distortion. The $^1A_1$ has the same configuration as the $^3A_1$, but the two unpaired electrons are antiparallel. By transferring an electron from $4b_1$ to $11a_1$, we obtain the 2^1A_1 closed-shell state. Overall, we can conclude that, for all low-energy anionic states, all the valence orbitals of oxygen are doubly occupied, implying that each oxygen atom in the cluster has an oxidation state of −2, while vanadium has an oxidation state of +3.

Analyzing the electronic leading configurations of the low-lying states of the neutral cluster reveals that the $^2A_1$ and $^2B_1$ low-energy states can both be obtained by removal of an electron from the $11a_1$ orbital of the anionic $^3A_1$ and $^3B_1$ states, respectively, which is mainly the 4s orbital of vanadium. As a direct consequence, vanadium exhibits an oxidation state of +4 in these low-energy states of the neutral cluster. A further analysis of their electronic configurations shows that they are two components of the $^2\Delta_g$ of the linear VO_2. A $^2\Delta_g$ that is split as a consequence of a Renner−Teller distortion, which is a second-order effect, is expected to be small. Note that the CASSCF wave functions show profound single-reference characters for the lowest-lying states of the $VO_2^{-/0}$ clusters. The reference weights of the leading configuration of $^3A_1$, $^3B_1$, $^2A_1$, and $^2B_1$ are 85%, 86%, 82%, and 83%, respectively. Consequently, all the electron detachment processes involving the $^3A_1$, $^3B_1$, $^2A_1$, and $^2B_1$ states must strictly follow the one-electron detachment rule. The CASSCF leading configurations in Table 2 leave no doubt that there is no one-electron detachment process that gives rise to $^2A_1$ from $^3B_1$ or that gives rise to $^2B_1$ from $^3A_1$. This means that it is impossible for both the $^2A_1$ and $^2B_1$ states to appear in the photoelectron spectra of VO_2^- if the anionic initial state is solely $^3B_1$ or $^3A_1$.

Experimental Photoelectron Spectra of VO_2^-. The photoelectron spectra of VO_2^- were reported for photon energies of 532 nm, 355 nm, 266, and 193 nm.[9] In Figure 3, we present the 193 nm photoelectron spectrum, which reveals X, A, B, and C bands at 2.03, 2.60, 4.00, and 4.60 eV, respectively. Specifically, for the X band, the 532 nm photoelectron spectrum, which can be seen in Figure 4a, shows a vibrational progression with a frequency of 970 ± 40 cm^{-1}. In addition to these bands, the 532 nm photoelectron spectrum presents two other weaker features, namely, a least-intense feature X′ at 1.72 eV and a broad unresolved X″ feature at 1.9 eV. In the same work and based on previous theoretical and experimental

dx.doi.org/10.1021/ct500526m | J. Chem. Theory Comput. 2014, 10, 4037−4044

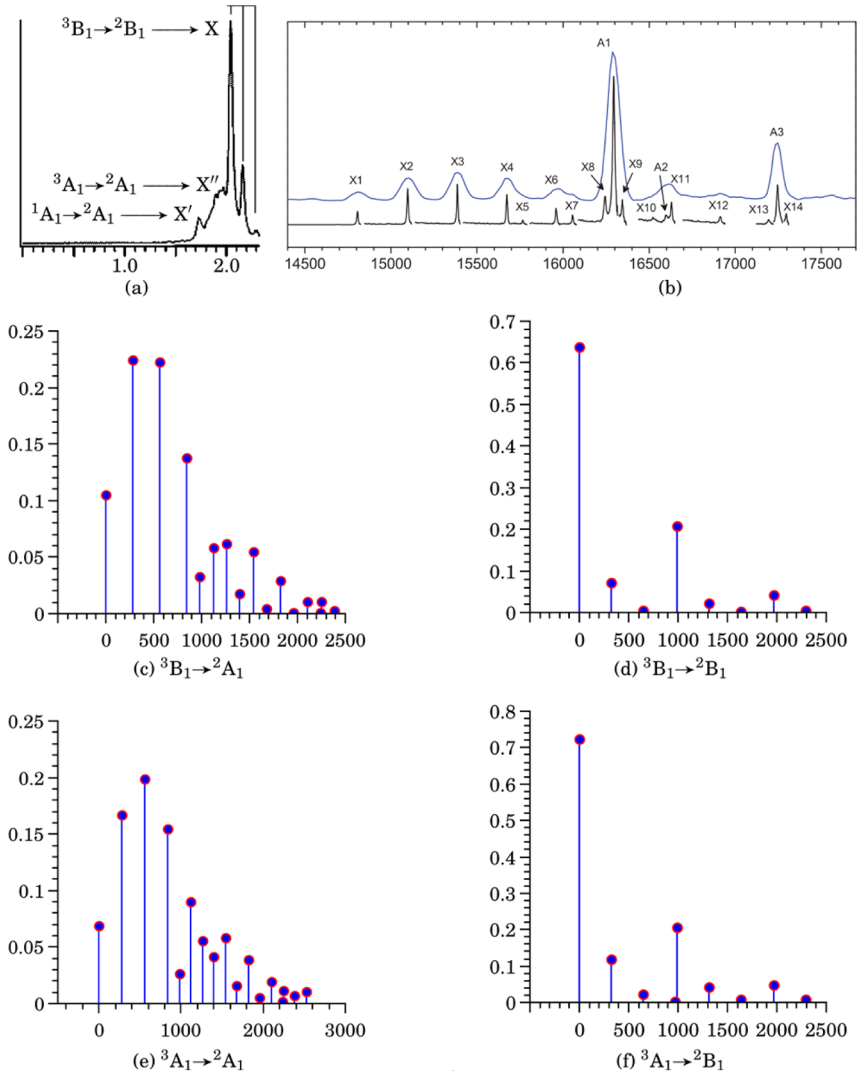

Figure 4. (a) The 532 nm photoelectron spectrum of VO_2^-.[9] Abscissa: binding energies in eV. Ordinate: arbitrary units for intensities. (b) High-resolution SEVI spectra for the low-energy part of the photoelectron spectra.[18] Abscissa: binding energies in wavenumbers. Ordinate: arbitrary units for intensities. The X and A bands correspond to the X″ and X bands of spectrum shown in (a), respectively. Franck−Condon factor for the $^3B_1 \rightarrow {}^2A_1$ (c), $^3B_1 \rightarrow {}^2B_1$ (d), $^3A_1 \rightarrow {}^2A_1$ (e), and $^3A_1 \rightarrow {}^2B_1$ (f) ionizations, as obtained with RCCSD(T).

studies on VO_2 that predicted the $^2A_1$ as its ground state,[7] the anionic ground state was thought to be the $^1A_1$ state with a closed-shell electronic structure. Therefore, the X, A, B, and C bands were, respectively, assigned to ionizations from $^1A_1$ to $^2A_1$, $^2B_1$, $^2B_2$, and $^2A_2$, while the X′ and X″ features were suggested to be the result of ionizations from unidentified excited states of VO_2^-. The vibrational progression of 970 cm^{-1} of the X band was proposed to be the result of the slight change in the V−O bond distance between the $^1A_1$ and $^2A_1$. The frequency of this progression was argued to be quite compatible with the value of 946 cm^{-1} for the V−O symmetric vibrational mode as indicated by matrix Fourier transform infrared spectroscopy (FTIR) measurements.[5] Moreover, all peaks in the vibrational progression of the X band are very sharp, implying that there is no contribution of the OVO bending mode with a too-small frequency to be resolved. As a result, the OVO bond angle was predicted as almost unchanged under the ionization.

Very recently, Neumark and co-workers confirmed this finding by reporting high-resolution SEVI spectra for the low-energy part of the photoelectron spectrum of VO_2^-.[18] The detachment energies for their X, A, (Figure 4b) and B bands correspond reasonably well with the values of the X″, X, and A bands of the 532 nm spectrum of the previous experimental study,[9] but a different interpretation was given; therefore, a different labeling scheme was used in these two studies. On the basis of BPW91 calculations, the $^3B_1$ state was predicted as the ground state of the anion with the $^3A_1$ state 0.07 eV less stable. This energy gap was considered to be sufficiently large enough to assign the recorded high-resolution spectra by using the $^3B_1$ ground state as the underlying initial state for all observed bands. On the basis of the computed BPW91 Franck−Condon factors, the vibrational X progression was assigned to the electronic $^3B_1 \rightarrow {}^2A_1$ transition, which rather surprisingly is not a one-electron detachment process. The multireference character of these states was invoked to explain this assignment but was not proven. Especially, the most-intense X3 peak in the corresponding experimental vibrational progression could only be reproduced for the electronic $^3B_1 \rightarrow {}^2A_1$ transition and not for that of the $^3A_1 \rightarrow {}^2A_1$ transition, which potentially can be a one-electron detachment transition. However, our calculations point to single-reference character of the involved states. Also,

dx.doi.org/10.1021/ct500526m | J. Chem. Theory Comput. 2014, 10, 4037−4044

our RCCSD(T) calculations predict a near-degeneracy of the $^3B_1$ and $^3A_1$ states, with an energy difference 0.02 eV, which is smaller than the 0.12 eV zero-point vibration energy, as can be estimated from the harmonic vibrational frequencies. This allows a population of the excited $^3A_1$ state, making the latter transition plausible as the underlying ionization process for the X vibrational progression. Therefore, it is absolutely necessary to re-examine the previously made assignments for all features in the photoelectron spectra of VO_2^- by using the highly accurate ab initio RCCSD(T) method for calculating the detachment energies and the vibrational progressions.

Assignment of the Low-Energy Bands: Detachment Energies. From the above discussion on the low-lying states of $VO_2^{-/0}$, it was concluded that it is very difficult to identify the ground state of both the anionic and neutral cluster because of a near degeneracy of the anionic $^3B_1$, $^3A_1$, and $^1A_1$ states and of the neutral $^2B_1$ and $^2A_1$ states. Therefore, it is essential to find out the contribution of all these low-lying states to the X, X″, and X′ features in the 532 nm photoelectron spectrum. On the basis of the electronic configurations of the three lowest states, there are an equal number of possible one-electron detachment processes that can give rise to the lowest binding energy bands of the spectrum: $^3B_1 \rightarrow {}^2B_1$, $^3A_1 \rightarrow {}^2A_1$, and $^1A_1 \rightarrow {}^2A_1$. For all these transitions an electron is removed from the $11a_1$ orbital, which has its main contribution from the 4s orbital of vanadium. The CASPT2 results for the low-lying states in Table 2 estimate the corresponding adiabatic detachment energies as 1.75 eV for $^3B_1 \rightarrow {}^2B_1$, 1.69 eV for $^3A_1 \rightarrow {}^2A_1$, and 1.65 eV for $^1A_1 \rightarrow {}^2A_1$. A first comparison of these theoretical ADEs with the experimental electron binding energies for the X, X″, and X′ bands of 2.03, 1.90, and 1.72 eV of the 532 nm spectrum[9] or the 2.0202 and 1.8357 eV ADEs of the SEVI spectrum[18] indicates that the former values are calculated too small by an amount of 0.2 to 0.3 eV. This is the outcome of the expected larger quantity of electron correlation present in the anion because of its extra electron and the well-known fact that CASPT2 with, for practical reasons, a limited active space is not capable enough to recover the dynamical correlation energy to a level comparable to the experimental accuracy reached in the photoelectron spectra. From Table 1 the following RCCSD(T) ADEs of 2.00 eV ($^3B_1 \rightarrow {}^2B_1$) and 1.86 eV for the ($^3A_1 \rightarrow {}^2A_1$) are easily derived, which correspond to within 0.04 eV or less with the experimental data. This illustrates once again that RCCSD(T) is superior for calculating low-energy states.

However, the sequence of the calculated detachment energies suggests that $^3B_1$ is the anionic ground state giving rise as its initial state to the most intense band of the lower energy bands, namely, the X band of the 532 nm spectrum (Figure 4a) or the A band of the SEVI spectrum in Figure 4b, which consequently corresponds to the transition $^3B_1 \rightarrow {}^2B_1$. Indeed, although the $^3A_1$ state is computed to be 0.07 eV more stable than the $^3B_1$ state at the CASPT2 level, it is calculated to be scarcely 0.02 eV less stable by RCCSD(T). Further, the lower intensity of the X″ feature compared to that of the X band can now be understood, since it originates from the anionic first excited state $^3A_1$ as its initial state and has the neutral ground state $^2A_1$ as the final state of this ionization. Further on, the intensity of the lowest energy band X′ is in turn lower than that of the X″ band, which agrees with the fact that it is predicted to possess the ionic second excited state $^1A_1$ as its initial state. Because this band is, on the basis of the one-electron rule, found to also have the neutral $^2A_1$ ground state as the final state, the corresponding detachment energy is accordingly lower than that of the X″ band. In summary, for the low-energy part of the photoelectron spectrum and completely on the basis of the relative energies calculated by CASPT2 and RCCSD(T), it is possible to assign the transitions $^3B_1 \rightarrow {}^2B_1$, $^3A_1 \rightarrow {}^2A_1$, and $^1A_1 \rightarrow {}^2A_1$ to the X (A band of the SEVI spectra), X″ (X band in the SEVI spectra), and the X′ features of the 532 nm spectrum, respectively. Because of the expected error bars of the computational methods and the rather small differences in detachment energies, supplemental theoretical confirmation of these assignments is undoubtedly needed. Additionally, our assignment for the X band progression of the SEVI spectra differs from the assignment made in ref 18 and therefore needs further consideration.

Assignment of the Low-Energy Bands: Franck–Condon Simulations. So, with the purpose to further ensure our assignment for the low-energy features of the photoelectron spectra of the VO_2^- cluster, Franck–Condon factors were derived based on the RCCSD(T) geometries, vibrational frequencies, and vibrational normal modes for the $^3B_1 \rightarrow {}^2A_1$ (Figure 4c), $^3B_1 \rightarrow {}^2B_1$ (Figure 4d), $^3A_1 \rightarrow {}^2A_1$ (Figure 4e), and $^3A_1 \rightarrow {}^2B_1$ (Figure 4f) ionizations. As can be seen in Figure 4d, the $^3B_1 \rightarrow {}^2B_1$ transition shows as a one-electron detachment a simple vibrational progression with two sharp peaks, which is in good agreement with the composition of the X band in Figure 4a and the A band of the high-resolution spectrum of Figure 4b. A closer analysis shows that the theoretical progression is entirely due to the symmetric V–O stretching normal mode with a spacing of 986 cm^{-1} that moreover corresponds well with the experimental measured frequencies of 970 ± 40 cm^{-1} and 952 cm^{-1} in Figure 4a,b, respectively. The RCCSD(T) data in Table 1 reveal a noticeable change in the V–O bond distance during this ionization, from 1.651 Å in $^3B_1$ to 1.620 Å in $^2B_1$, while at the same time the OVO bond angle remains almost unchanged, that is, 122.09° in $^3B_1$ and 120.83° in $^2B_1$. This explains the symmetric stretching normal mode contribution to the progression and the absence of the symmetric bending normal mode with a frequency of 324 cm^{-1}. The Franck–Condon simulation for the $^3A_1 \rightarrow {}^2A_1$ ionization is represented in Figure 4e. Now, in addition to the vibrational progression of the symmetric V–O stretching mode of 984 cm^{-1}, there are also observable contributions predicted from the OVO bending mode with a frequency of 280 cm^{-1}. This can be explained by the fact that for this ionization process both the V–O bond distance and OVO bond angle undergo considerable changes from 1.654 Å and 123.70° in $^3A_1$ to 1.617 Å and 113.59° in $^2A_1$. This vibrational analysis, therefore, proposes an unresolved broad band for this ionization, which is in sharp contrast with the three sharp peaks constituting the experimental value of the X band in Figure 4a and the measured progression of the A band in Figure 4b. It is more appropriate to ascribe this ionization to the vibrational unresolved X″ band (Figure 4a). Moreover, the simulated progression of the $^3A_1 \rightarrow {}^2A_1$ ionization in Figure 4e is in very good agreement with the recorded experimental progression of the X band in the SEVI spectra. Indeed, in Figure 4b the X3 peak is the most intense transition, which is in full agreement with the calculated Franck–Condon factors for the $^3A_1 \rightarrow {}^2A_1$ ionization (Figure 4e) but in disagreement with the simulated progression for the $^3B_1 \rightarrow {}^2A_1$ ionization (Figure 4c). In conclusion, our Franck–Condon factor simulations successfully reproduce the vibrational progression of the X and A progressions of the high-resolution SEVI spectra[18] and thus confirm our proposed

assignment on the basis of the RCCSD(T) and CASPT2 detachment energies, which ascribed the $^3B_1 \rightarrow {}^2B_1$ transition to the A band and the $^3A_1 \rightarrow {}^2A_1$ transition to the X band of Figure 4b or the X band and X″ bands of the 532 nm spectra in Figure 4a, respectively.

To summarize, our assignment of the low-lying bands in the photoelectron spectra of VO_2^- is in close agreement with the interpretation of Neumark and co-workers for their high-resolution spectra.[18] The ground state of anionic cluster is characterized by us as $^3B_1$, and it is consequently used as the initial state to explain the principal bands in the spectra. The three lowest bands are assigned to the transitions to the $^2A_1$, $^2B_1$, and 2^2A_1 states. However, because the $^3B_1 \rightarrow {}^2A_1$ transition is not a one-electron detachment process, we propose to use the $^3A_1 \rightarrow {}^2A_1$ transition to explain the lowest energy band in the high-resolution spectra. In this work, the energies of the $^3A_1$ and $^3B_1$ states are calculated to differ only 0.02 eV by RCCSD(T) and 0.07 eV by CASPT2. Such near degeneracy, which is less than the zero-point vibrational energy, is the reason why both of these two states are populated in the experiment even at very low temperatures. Even further, the X′ band, which is only present in the 532 nm photoelectron spectrum of Wang and co-workers,[9] should be ascribed to the second excited anionic state $^1A_1$, which has the same electronic configuration as $^3A_1$ and which is most likely also to be populated. According to the CASPT2 results of Table 2 it is just 0.03 eV less stable than the $^3B_1$ anionic ground state. Consequently, the transition from this singlet state to the $^2A_1$ neutral ground state of the neutral cluster can as a one-electron detachment process be assigned to the lowest energy X′ band in the 532 nm spectrum. In general, we propose that the anionic ground state is the $^3B_1$ state, while the first excited $^3A_1$ anionic state is also populated in the high-resolution photoelectron spectra.

Assignment of the 193 nm Spectrum. Having established firmly the true ground state of the anionic VO_2^- cluster, it was used subsequently as the initial state for the assignment of the high-energy and high-intensity part of the 193 nm photoelectron spectrum in Figure 3. The A band starting at 2.60 eV is proposed to correspond to the transition $^3B_1 \rightarrow 2^2A_1$, which involves a one-electron detachment from the $4b_1$ (d_{xz}) orbital. The ADE of this ionization as predicted at the CASPT2 level in Table 2 is 2.27 eV, which is somewhat smaller than the experimental value. The RCCSD(T) VDE in Table 1 of 2.86 eV for the $^3B_1 \rightarrow 2^2A_1$ ionization is unquestionably in better agreement with experiment. Exclusively on the basis of the CASPT2 data in Table 2, the B and C bands of the 193 nm spectrum are assigned to the removal of an electron from one of the oxygen orbitals. The B band with an experimental electron binding energy of 4.0 eV is assigned to the transition from $^3B_1$ to both the $^4A_2$ and $^2A_2$ states, during which in both cases an electron is removed from the $6b_2$ orbital. Indeed, according to Table 2 the $^4A_2$ and $^2A_2$ states possess the same leading electronic configurations. From Figure 2 the $6b_2$ orbital is mainly composed of 2p orbitals on oxygen. The calculated vertical detachment energies (VDEs) for these two ionizations amount to 4.14 and 4.12 eV, which are in good agreement with the experimental value. The C band at 4.6 eV is the result of the removal of an electron from the $9a_1$ orbital of the $^3B_1$ state. This ionization process gives rise to the high-spin $^4B_1$ and low-spin 2^2B_1 states. And again, the CASPT2 calculation affords very comparable VDEs to the experiment, namely, 4.58 eV for the $^3B_1 \rightarrow {}^4B_1$ transition and 4.55 eV for the $^3B_1 \rightarrow 2^2B_1$ transition.

CONCLUSION

By investigating the highly complicated electronic structures of the $VO_2^{-/0}$ clusters, a novel global assignment is proposed for all peaks and bands in the photoelectron spectra of VO_2^-. CASPT2 and RCCSD(T) calculations predict a near-degeneracy of three states ($^3B_1$, $^3A_1$, and $^1A_1$) for the anionic cluster and of two states ($^2B_1$ and $^2A_1$) for the neutral cluster. On the basis of the electronic leading configuration of the low-lying states of $VO_2^{-/0}$, we suggest an oxidation state of +3 or +4 for vanadium and −2 for each oxygen. The interpretation of the main features of the photoelectron spectra of VO_2^- (X, A to C bands in the 193 nm spectrum) is based on the $^3B_1$ anionic ground state. The X band is identified as the result of the $^3B_1 \rightarrow {}^2B_1$ transition, while the lower-intensity X′ and X″ features of the 532 nm spectrum are assigned as ionizations starting from the low-lying anionic excited $^1A_1$ and $^3A_1$ states. They correspond to the $^1A_1 \rightarrow {}^2A_1$ and $^3A_1 \rightarrow {}^2A_1$ ionizations, respectively. Common for these three low-energy ionizations, an electron is detached from the $11a_1$ (mainly 4s of vanadium) orbital. The Franck−Condon factor simulations for the $^3A_1 \rightarrow {}^2A_1$ and $^3B_1 \rightarrow {}^2B_1$ ionizations successfully reproduce the peaks in the vibrational progression of the SEVI X and A vibrational progressions, respectively. The A band of the 193 nm spectrum, that is, the B band of the SEVI spectra, is in essence an ionization from the $^3B_1$ state to the 2^2A_1 state. All these features of the spectra involve mainly a detachment of an electron from an orbital with predominantly metal 4s or 3d character. The higher-energy B and C bands in the 193 nm spectrum, on the other hand, are suggested to be the results of the ionizations of electrons out of orbitals mainly centered on oxygen. The initial state for these two bands is always the $^3B_1$ anionic ground state. In particular, the B band corresponds to the ionization of an electron from the $6b_2$ orbital, which results in the high-spin $^4A_2$ and the low-spin $^2A_2$ states. The C band is attributed to the transitions to the $^4B_1$ and 2^2B_1 states, in which an electron from the $9a_1$ orbital is removed.

AUTHOR INFORMATION

Corresponding Author

*E-mail: marc.hendrickx@chem.kuleuven.be.

Notes

The authors declare no competing financial interest.

REFERENCES

(1) Deo, G.; Wachs, I. E. Reactivity of Supported Vanadium Oxide Catalysts—The Partial Oxidation of Methanol. *J. Catal.* **1994**, *146*, 323−334.

(2) Guimond, S.; Abu Haija, M.; Kaya, S.; Lu, J.; Weissenrieder, J.; Shaikhutdinov, S.; Kuhlenbeck, H.; Freund, H. J.; Dobler, J.; Sauer, J. Vanadium Oxide Surfaces and Supported Vanadium Oxide Nanoparticles. *Top. Catal.* **2006**, *38*, 117−125.

(3) Weckhuysen, B. M.; Keller, D. E. Chemistry, Spectroscopy and the Role of Supported Vanadium Oxides in Heterogeneous Catalysis. *Catal. Today* **2003**, *78*, 25−46.

(4) Bond, G. C.; Tahir, S. F. Vanadium Oxide Monolayer Catalysts—Preparation, Characterization, and Catalytic Activity. *Appl. Catal.* **1991**, *71*, 1−31.

(5) Chertihin, G. V.; Bare, W. D.; Andrews, L. Reactions of Laser-Ablated Vanadium Atoms with Dioxygen. Infrared Spectra of VO, VO_2, $OOVO_2$, and V_2O_2 in Solid Argon. *J. Phys. Chem. A* **1997**, *101*, 5090−5096.

(6) Gutsev, G. L.; Rao, B. K.; Jena, P. Systematic Study of Oxo, Peroxo, and Superoxo Isomers of 3d-Metal Dioxides and Their Anions. *J. Phys. Chem. A* **2000**, *104*, 11961−11971.
(7) Knight, J. L. B.; Babb, R.; Ray, M.; Banisaukas Iii, T. J.; Russon, L.; Dailey, R. S.; Davidson, E. R. An Electron Spin Resonance Investigation of Vanadium Dioxide ($^{51}V^{16}O_2$ and $^{51}V^{17}O_2$) and $^{51}V^{17}O$ in Neon Matrices with Preliminary Assignments for VO_3 and V_2^+: Comparison with Ab Initio Theoretical Calculations. *J. Chem. Phys.* **1996**, *105*, 10237−10250.
(8) Uzunova, E. L.; Mikosch, H.; St. Nikolov, G. Electronic Structure of Oxide, Peroxide, and Superoxide Clusters of the 3d Elements: A Comparative Density Functional Study. *J. Chem. Phys.* **2008**, *128*, 094307−094312.
(9) Wu, H.; Wang, L.-S. A Photoelectron Spectroscopic Study of Monovanadium Oxide Anions (VO_x^-, x = 1−4). *J. Chem. Phys.* **1998**, *108*, 5310−5318.
(10) Wang, H. Q.; Li, H. F. Probing the Structural and Electronic Properties of Small Vanadium Dioxide Clusters by Density Functional Theory and Comparison with Experimental Photoelectron Spectroscopy. *J. Chem. Phys.* **2012**, *137*.
(11) Wang, H.-Q.; Li, H.-F.; Kuang, X.-Y. Probing the Structural and Electronic Properties of Small Vanadium Monoxide Clusters. *Phys. Chem. Chem. Phys.* **2012**, *14*, 5272−5283.
(12) Uzunova, E. L. Electronic Structure of Trioxide, Oxoperoxide, Oxosuperoxide, and Ozonide Clusters of the 3d Elements: Density Functional Theory Study. *J. Phys. Chem. A* **2011**, *115*, 1320−1330.
(13) Gong, Y.; Zhou, M. F.; Andrews, L. Spectroscopic and Theoretical Studies of Transition Metal Oxides and Dioxygen Complexes. *Chem. Rev. (Washington, DC, U. S.)* **2009**, *109*, 6765−6808.
(14) Miliordos, E.; Mavridis, A. Electronic Structure of Vanadium Oxide. Neutral and Charged Species, $VO^{0,\pm}$. *J. Phys. Chem. A* **2007**, *111*, 1953−1965.
(15) Pykavy, M.; van Wullen, C. Multireference Correlation Calculations for the Ground States of $VO^{+/0/-}$ Using Correlation Consistent Basis Sets. *J. Phys. Chem. A* **2003**, *107*, 5566−5572.
(16) Zhai, H. J.; Wang, L. S. Electronic Structure and Chemical Bonding of Divanadium-Oxide Clusters (V_2O_x, x = 3−7) from Anion Photoelectron Spectroscopy. *J. Chem. Phys.* **2002**, *117*, 7882−7888.
(17) Pramann, A.; Koyasu, K.; Nakajima, A.; Kaya, K. Anion Photoelectron Spectroscopy of $V_nO_m^-$ (n = 4−15; m = 0−2). *J. Chem. Phys.* **2002**, *116*, 6521−6528.
(18) Kim, J. B.; Weichman, M. L.; Neumark, D. M. Vibronic Structure of VO_2 Probed by Slow Photoelectron Velocity-Map Imaging Spectroscopy. *J. Chem. Phys.* **2014**, *140*, 034307.
(19) Hendrickx, M. F. A.; Tran, V. T. On the Electronic and Geometric Structures of $FeO_2^{-/0}$ and the Assignment of the Anion Photoelectron Spectrum. *J. Chem. Theory Comput.* **2012**, *8*, 3089−3096.
(20) Tran, V. T.; Hendrickx, M. F. A. Description of the Geometric and Electronic Structures Responsible for the Photoelectron Spectrum of FeO_4^-. *J. Chem. Phys.* **2011**, *135*, 094505.
(21) Tran, V. T.; Hendrickx, M. F. A. A CASPT2 Description of the Electronic Structures of $FeO_3^{-/0}$ in Relevance to the Anion Photoelectron Spectrum. *J. Chem. Theory Comput.* **2011**, *7*, 310−319.
(22) Tran, V. T.; Hendrickx, M. F. A. Assignment of the Photoelectron Spectra of $FeS_3^{-/0}$ by Density Functional Theory, CASPT2, and RCCSD(T) Calculations. *J. Phys. Chem. A* **2011**, *115*, 13956−13964.
(23) Roos, B. O.; Lindh, R.; Malmqvist, P.-Å.; Veryazov, V.; Widmark, P. O. New Relativistic ANO Basis Sets for Transition Metal Atoms. *J. Phys. Chem. A* **2005**, *109*, 6575−6579.
(24) Roos, B. O.; Lindh, R.; Malmqvist, P.-Å.; Veryazov, V.; Widmark, P. O. Main Group Atoms and Dimers Studied with a New Relativistic ANO Basis Set. *J. Phys. Chem. A* **2004**, *108*, 2851−2858.
(25) Reiher, M.; Wolf, A. Exact Decoupling of the Dirac Hamiltonian. II. The Generalized Douglas-Kroll-Hess Transformation up to Arbitrary Order. *J. Chem. Phys.* **2004**, *121*, 10945−10956.
(26) Reiher, M.; Wolf, A. Exact Decoupling of the Dirac Hamiltonian. I. General Theory. *J. Chem. Phys.* **2004**, *121*, 2037−2047.
(27) Ishikawa, Y.; Vilkas, M. J. Relativistic Quantum Mechanics of Many-Electron Systems. *J. Mol. Struct.: THEOCHEM* **2001**, *573*, 139−169.
(28) Karlström, G.; Lindh, R.; Malmqvist, P.-Å.; Roos, B. O.; Ryde, U.; Veryazov, V.; Widmark, P. O.; Cossi, M.; Schimmelpfennig, B.; Neograd, P.; Seijo, L. MOLCAS: a Program Package for Computational Chemistry. *Comput. Mater. Sci.* **2003**, *28*, 222−239.
(29) Becke, A. D. Density-Functional Exchange-Energy Approximation with Correct Asymptotic Behavior. *Phys. Rev. A* **1988**, *38*, 3098−3100.
(30) Becke, A. D. Density-Functional Thermochemistry 0.3. The Role of Exact Exchange. *J. Chem. Phys.* **1993**, *98*, 5648−5652.
(31) Lee, C. T.; Yang, W. T.; Parr, R. G. Development of the Colle−Salvetti Correlation-Energy Formula into a Functional of the Electron-Density. *Phys. Rev. B* **1988**, *37*, 785−789.
(32) Perdew, J. P. Density-Functional Approximation for the Correlation-Energy of the Inhomogeneous Electron-Gas. *Phys. Rev. B* **1986**, *33*, 8822−8824.
(33) Weigend, F.; Ahlrichs, R. Balanced Basis Sets of Split Valence, Triple Zeta Valence and Quadruple Zeta Valence Quality for H to Rn: Design and Assessment of Accuracy. *Phys. Chem. Chem. Phys.* **2005**, *7*, 3297−3305.
(34) Balabanov, N. B.; Peterson, K. A. Systematically Convergent Basis Sets for Transition Metals. I. All-Electron Correlation Consistent Basis Sets for the 3d Elements Sc−Zn. *J. Chem. Phys.* **2005**, *123*, 064107.
(35) Borrelli, R.; Peluso, A. Dynamics of Radiationless Transitions in Large Molecular Systems: A Franck-Condon-Based Method Accounting for Displacements and Rotations of all the Normal Coordinates. *J. Chem. Phys.* **2003**, *119*, 8437−8448.
(36) Werner, H.-J.; Knowles, P. J.; Manby, F. R.; Schütz, M.; et al. *MOLPRO, Version 2009.1, a Package of Ab Initio Programs,* see http://www.molpro.net (accessed September 2011).